JNC TN8400 2000－015

電磁遷移確率の厳密解とFPアイソマー準位遷移確率に関する研究

（研究報告）

2000年3月

核燃料サイクル開発機構
東海事業所

Ⓣ

JNC TN8400 2000－015
２０００年３月

電磁遷移確率の厳密解と FPアイソマー準位遷移確率に関する研究

[研究報告]

和田　浩明*

要　旨

本報告は，博士研究員として平成９年10月から平成12年３月までに行なった研究内容をまとめたものである。本報告は、大きく２つの内容に分かれている。すなわち、１つは、高エネルギー光による電磁遷移過程の遷移率の厳密解を求める研究である。２つめの研究は、^{137}Cs(n,γ)^{138}Cs 熱中性子吸収反応で ^{138}Cs のアイソマー（^{138m}Cs）が生成される確率の測定である。

1) 最近の高エネルギービーム技術の発展により、高エネルギー光の研究に対する関心が高まっている。本研究では、高エネルギー光に対する電気的遷移（*El* 遷移）の遷移率を定式化した。遷移率を計算する際には、電場の表式は長波長近似しないで厳密なものを使い、原子核の波動関数として調和振動子型波動関数を使った。

2) 放射性核種 ^{137}Cs の熱中性子吸収断面積を高精度化するため、^{137}Cs(n,γ)^{138}Cs 反応で ^{138m}Cs が生成される確率を測定し、^{138m}Cs 生成の寄与を含む断面積を求めた。^{138g}Cs と ^{138m}Cs の両方の崩壊から放射される 1436keV γ 線の時間変化から、^{138g}Cs と ^{138m}Cs が熱中性子吸収反応で生成される割合を求めた。その結果、^{138m}Cs が生成される確率は 0.75±0.18 となった。この場合、^{138m}Cs 生成が熱中性子吸収断面積に与える寄与はこれまでの実験値を 9±2%上方修正させ、熱中性子吸収断面積として σ_0=0.27±0.03 b が得られた。

---

* 環境保全･研究開発センター
先進リサイクル研究開発部　先進リサイクル解析評価 Gr

JNC TN8400 2000－015
March, 2000

Exact Solution of Electric Transitions and Production Probability of Isomer State of FP

Hiroaki Wada*

Abstract

This report describes the study done within the period of time when I was postdoctoral research worker at Japan Nuclear Cycle Development Institute. The report includes two parts as follows.

1) Exact Solution of Electric Transitions for High Energy photons

Technologies for creating high-energy γ beams have been rapidly developed. These advancements make the research using high-energy γ-rays more important. The electric transition rates for high energy γ-rays were formulated. The electric multipole fields were treated strictly in the process of calculating the electric transition rates and the nuclear states were taken as the harmonic oscillator wave functions.

2) Production of the isomeric state of ^{138}Cs in the thermal neutron capture reaction $^{137}Cs(n,\gamma)^{138}Cs$

In order to obtain precise data of the neutron capture cross section of the reaction $^{137}Cs(n,\gamma)^{138}Cs$, the production probability of isomer state ^{138m}Cs was measured in this work. The 1436keV γ-ray emitted from both of ^{138g}Cs and ^{138m}Cs was measured. A production ratio of ^{138m}Cs to (^{138g}Cs and ^{138m}Cs) was deduced from time dependence of peak counts of 1436keV γ-ray. The probability of the production of ^{138m}Cs was obtained as 0.75 ± 0.18 and this value revised the effective cross section upwards $9\pm2\%$. The effective cross section $\hat{\sigma}$ and the thermal neutron capture cross section σ_0 were obtained as $\hat{\sigma}=0.29\pm0.02$ b and $\sigma_0=0.27\pm0.03$ b with taking into account the production of ^{138m}Cs.

* Advanced Fuel Recycle Technology Division
Recycle System Analysis Group

目　次

第１章　研究の概要

1.1 高エネルギー光による電磁遷移過程の遷移率の厳密解

核データの高精度な理論的予測は、先進的核燃料サイクルの開発を進めるうえで重要である。とくに最近、ビーム技術が急速な発展を遂げており、これを先進的核燃料サイクルに効率よく取り入れることが期待される。そのためには、広範囲のエネルギー領域での量子ビームと物質との相互作用を核反応理論によって正確に予測することが重要である。ところが、高い入射エネルギーのガンマ線による、重い原子核の光核反応断面積を精度良く理論的に予測することは非常に困難である。その原因の一つには、計算の簡単化のために広く用いられている長波長近似の精度が悪いためである。長波長近似できるための条件は$kR \ll 1$であるのに対して、高いエネルギー領域では$kR \geq 1$となることから、長波長近似を使わない解析をしなくてはならない。ここで、kとRはそれぞれ、光の波数と光と相互作用する系の典型的な長さ(原子や原子核の半径等)を表す。

本研究では，光吸収による電気的遷移（El遷移）の遷移率(単位時間あたりの遷移確率)を，調和振動子波動関数を使って長波長近似せず定式化した。El遷移の行列要素の表式は

$$M_{fi}(k\mu;El) = -\frac{\sqrt{2\pi}i^{l+1}\sqrt{2l+1}}{k\sqrt{l(l+1)}}\{\int d^3r < f(t)|\hat{\mathbf{j}}(\mathbf{r})|i(t)> \cdot\nabla[(1+r\frac{\partial}{\partial r})j_l(kr)Y_{l\mu}(\theta,\phi) + k^2\int d^3r\,\mathbf{r}\cdot< f(t)|\hat{\mathbf{j}}(\mathbf{r})|i(t)> j_l(kr)Y_{l\mu}(\theta,\phi)\}e^{-i\omega t} \quad (1)$$

である。ここで、lは多重極展開された電場の軌道角運動量を表す。長波長近似($kR \ll 1$)では、(1)式の第２項は第１項に比べて非常に小さいので無視できる。しかし、$kR \geq 1$となる高エネルギー領域では、(1)式の両方の項を計算せねばならない。本研究では，(1)式の行列要素に調和振動子型波動関数を代入して、(1)の第２項を無視せずに計算した。得られた結果は厳密な計算結果なので，広いエネルギー範囲の光および，さまざまな質量の原子核に対して正しい結果を与える。

研究の詳細は，別添えの報告書としてまとめた(第２章の2.1)。そこでは、原子核の独立単一粒子模型に基づき、調和振動子の$1s$状態からnlへと移るEl過程の遷移率の計算結果を示した。具体的には、El遷移の遷移率の光エネルギーによる変化を調べた。さらに、得られた結果とWeisskopfによる長波長近似した遷移率(原子核内で一定な波動関数を使用)との比較も行なった。

1.2 $^{137}Cs(n,\gamma)^{138}Cs$ 熱中性子吸収反応における ^{138}Cs アイソマー (^{138m}Cs) の生成確率

中性子吸収反応を利用した核分裂生成物を核変換する技術を確立していくうえで，核データの整備は重要である。本研究では，放射性核種 ^{137}Cs に中性子の熱中性子吸収断面積を高精度化するために，$^{137}Cs(n,\gamma)^{138}Cs$ 反応で ^{138m}Cs (^{138}Cs のアイソマー) が生成される確率を測定し，^{138m}Cs 生成の寄与を含む断面積を求めた。照射試料は約 0.37MBq の ^{137}Cs を使い,京都大学原子炉実験所の圧気輸送管 Pn-3 で中性子を 3 分間照射した。^{138g}Cs(^{138}Cs の基底準位)と ^{138m}Cs の半減期がそれぞれ 33.41 分と 2.91 分と異なることを利用して、^{138g}Cs と ^{138m}Cs の両方が ^{138}Ba へと β^- 崩壊する過程で放出される 1436keV γ 線の時間変化から,^{138g}Cs と ^{138m}Cs が熱中性子吸収反応で生成される割合を求めた。その結果,$^{137}Cs(n,\gamma)^{138}Cs$ 反応で生成される ^{138}Cs のうち,^{138m}Cs が生成される確率は 0.75±0.18 となった。この場合,^{138m}Cs 生成が熱中性子吸収断面積に与える寄与はこれまでの実験値を 9±2%上方修正させ,$^{137}Cs(n,\gamma)^{138}Cs$ 反応の熱中性子吸収断面積として σ_0=0.27±0.03 b (実効断面積は σ=0.29±0.02 b)が得られた。

研究の詳細は,別添えの報告書(第 2 章の 2.2)としてまとめ, Journal of Nuclear Science and Technology に投稿した。

第２章　研究の詳細

2.1　Exact Solution of Electric Transitions for High Energy photons

Exact Solution of Electric Transitions for High Energy photons

Hiroaki Wada and Hideo Harada
Japan Nuclear Cycle Development Institute (JNC),
Tokai-mura, Naka-gun, Ibaraki-ken 319-1194

Abstract

The electric transition rates for high energy γ-rays are formulated and obtained numerically. The electric multipole fields are treated strictly in the process of calculating the electric transition rates and the nuclear states are taken as the harmonic oscillator wave functions. The electric transition rates between the $1s$ and the excited nl states are calculated without the long-wavelength approximation (LWA) and compared with the Weisskopf's estimates in case of $E1$, $E2$ and $E3$. The calculated transition rates are much smaller than the Weisskopf units for high energy photons. The results are used for the order of estimates of electric transition rates at the energy region where LWA is not valid.

1 Introduction

Technologies for creating high-energy γ beams have been rapidly developed (e.g. powerful synchrotron radiation facilities and γ ray beams by inverse compton scattering, etc.). These advancements make the research using high-energy γ-rays more important. Using the high-energy γ-rays and X-rays, the progress is being developed in the fields of nuclear and atomic physics, respectively.

A method of the long-wavelength approximation (LWA) has been applied to calculations of the nuclear photo effects (e.g. calculations of γ-transition, the giant dipole resonance, etc.) and calculations of the atomic photo effects (e.g. calculations of X-ray absorption fine structure, etc.). The LWA is nearly accurate under the condition $|\mathbf{k}|R \ll 1$ where $\mathbf{k}$ means wave vector of photon and R is radius of nucleus (or atom). This paper aims to provide exact electric transition operators that are even valid for the case of $|\mathbf{k}|R \gtrsim 1$.

The error in calculation by using the LWA is not negligible under the condition $|\mathbf{k}|R \gtrsim 1$. For example, the LWA is not valid for the calculation of the differential cross sections of the $^{16}O(\gamma, N)$ reaction in a few tens of MeV. Contributions of $E1$ and $E2$ multipole operators to the differential cross sections were calculated within random phase approximation and Hartree-Fock approximation, where expressions of the electric multipole fields were chosen as strict form and the approximated form in the LWA. The errors induced by using the LWA became large for photon energy above about 40 MeV ($|\mathbf{k}|R \gtrsim 0.61$ in this case) [1]. As another example, the radiative widths of the M1 transition from excited ^{12}C (15.11 MeV excitation) to the ground state led to a deviation of about 2% ($|\mathbf{k}|R = 0.21$ in this case) by using the LWA, where the matrix elements of magnetic multipole operators were expanded by the Fourier-Bessel series. The spherical Bessel functions were expanded into a power series in $|\mathbf{k}|R$ and the leading term is keeped in the LWA [2].

Weisskopf suggested the transition rates in the LWA with a single nucleon state for the order-of-magnitude estimations [3]. In these estimations, the wave functions are described by a constant radial wave function inside nuclei (vanishing outside nuclei) and spherical harmonic functions $Y_{lm}(\theta, \phi)$. These wave functions represent that the probability of proton is uniform in spherical nuclei. The transition rates between the ground state with $l = 0$ (s state) and the excited state with $l \neq 0$ are conveniently and widely used as the units (Weisskopf units) of the electric and magnetic transition rates. However, Weisskopf units do not give valid results for high energy photons or heavy nucleus ($|\mathbf{k}|R \gtrsim 1$) because Weisskopf units are calculated by using the LWA ($|\mathbf{k}|R \ll 1$). It is expected to obtain the valid transition rates for high photon energies and heavy nuclear masses with the simple evaluation forms as given by Weisskopf.

In this work, we restrict ourselves to El transitions and treat the electric multipole operators strictly without the calculations by using the LWA. The nuclear states are assumed as single-particle proton states that are the energy eigenfunctions of the spherical harmonic oscillator, since the constant wave functions are not energy eigenfunctions and are inappropriate to be used in calculating the transition rates in the case of $|\mathbf{k}|R \gtrsim 1$. We estimate the transition rates of the El transitions from grand state $1s$ to the exited states for the absorption of photons as typical El transition processes (where freedom of spin is ignored) in similar way of Weisskopf's estimation methods.

Firstly, a derivation process of the El transition rates with harmonic oscillator wave functions is briefly followed in section 2. Next, the differences between the calculated transition rates and Weisskopf unit are shown in cases of $E1$, $E2$ and $E3$ transitions in section 3. We discuss the results in section 4 and summarize in section 5.

2 Formulation of the El transition rates

In this section, the formulation of the El transition rates with the electric multipole fields that are not approximated by using the LWA is surveied. The electric multipole field is expressed as

$$\mathbf{A}_{l\mu}(\mathbf{r};E) = \frac{-i}{\hbar|\mathbf{k}|\sqrt{l(l+1)}}\nabla\times\left[\hat{\mathbf{L}}j_l(|\mathbf{k}|r)Y_{l\mu}(\Omega)\right] \quad , \tag{1}$$

where $\hat{L}$ ($= \mathbf{r}\times\hat{\mathbf{p}} = -i\hbar\mathbf{r}\times\nabla$) denotes an orbital angular momentum operator. And $\mathbf{k}$ ($\mu = \pm 1$) indicates the wave vector (the polarization index) of the photon. Substituting the electric multipole field (1) for the El transition matrix element for γ absorption

$$M_{fi}(|\mathbf{k}|\mu;El) = -\sqrt{2\pi}i^{l+1}\sqrt{2l+1}\int d^3r\langle f(t)|\hat{\mathbf{j}}(\mathbf{r})|i(t)\rangle\cdot\mathbf{A}_{l\mu}(\mathbf{r};E)e^{-i\omega t} \tag{2}$$

and changing the expression of the El transition matrix element in a vector analysis, the El matrix element is splitted in two parts [4, 5, 6] as

$$\begin{aligned} M_{fi}(|\mathbf{k}|\mu;El) &= -\frac{\sqrt{2\pi}i^{l+1}\sqrt{2l+1}}{|\mathbf{k}|\sqrt{l(l+1)}}\Bigg\{ \\ &\int d^3r\langle f(t)|\hat{\mathbf{j}}(\mathbf{r})|i(t)\rangle\cdot\nabla\left[\left(1+r\frac{\partial}{\partial r}\right)j_l(|\mathbf{k}|r)Y_{l\mu}(\Omega)\right] \\ &+|\mathbf{k}|^2\int d^3r\mathbf{r}\cdot\langle f(t)|\hat{\mathbf{j}}(\mathbf{r})|i(t)\rangle j_l(|\mathbf{k}|r)Y_{l\mu}(\Omega)\Bigg\}e^{-i\omega t} \quad . \end{aligned} \tag{3}$$

By performing a partial integration (the surface term vanishes because the extent of the nuclear current distribution is finite) and using the continuity equation for the current

$$\begin{aligned} 0 &= \frac{\partial}{\partial t}\langle f(t)|\hat{\rho}(\mathbf{r})|i(t)\rangle + \nabla\cdot\langle f(t)|\hat{\mathbf{j}}(\mathbf{r})|i(t)\rangle \\ &= \frac{i}{\hbar}(E_f - E_i)\langle f(t)|\hat{\rho}(\mathbf{r})|i(t)\rangle + \nabla\cdot\langle f(t)|\hat{\mathbf{j}}(\mathbf{r})|i(t)\rangle \quad , \end{aligned} \tag{4}$$

the El transition matrix element is transformed into

$$
\begin{aligned}
M_{fi}(|\mathbf{k}|\mu; El) &= \frac{\sqrt{2\pi} i^l \sqrt{2l+1}}{\sqrt{l(l+1)}} \Bigg\{ \\
&\frac{E_f - E_i}{\hbar|\mathbf{k}|} e_p \int d^3r \psi_f^*(\mathbf{r},t)\psi_i(\mathbf{r},t) \left(1 + r\frac{\partial}{\partial r}\right) j_l(|\mathbf{k}|r) Y_{l\mu}(\Omega) \\
&-i|\mathbf{k}| \frac{e_p \hbar}{2M_p i} \int d^3r \mathbf{r} \cdot \left[\psi_f^*(\mathbf{r},t)\nabla\psi_i(\mathbf{r},t) - (\nabla\psi_f^*(\mathbf{r},t))\psi_i(\mathbf{r},t)\right] \\
&j_l(|\mathbf{k}|r) Y_{l\mu}(\Omega) \Bigg\} e^{-i\omega t} \quad . \qquad (5)
\end{aligned}
$$

The symbol M_p (e_p) indicates the mass (charge) of the proton.

In viewpoint of independent one-particle model, the wave function of the nuclear state is given by the wave function of the proton. We take the wave functions of the nuclear states as harmonic oscillator wave functions

$$
\psi_{nlm}(\mathbf{r},t) = \sqrt{2\alpha^3 \frac{n!}{[\Gamma(n+l+\frac{3}{2})]^3}} e^{-\frac{\alpha^2}{2}r^2} (\alpha r)^l L_n^{(l+\frac{1}{2})}(\alpha^2 r^2) Y_{lm}(\theta,\phi) e^{-iE_{nl}t/\hbar} \; . \qquad (6)
$$

The initial and final states are $1s$ state ($\psi_i = \psi_{000}$) and nl state ($\psi_f = \psi_{nlm}$), respectively. The constant α is defined as

$$
\alpha = \sqrt{\frac{M_p \omega_0}{\hbar}} \qquad (7)
$$

and ω_0 is the angular frequency of the oscillator. The energy eigenvalue of the harmonic oscillator wave function ψ_{nlm} (6) is

$$
E_{nl} = \frac{\hbar\omega_0}{2}(4n + 2l + 3) \; . \qquad (8)
$$

The matrix element between $1s$ and nl states is

$$
\begin{aligned}
M_{fi}^{(H.O.)}(|\mathbf{k}|\mu; El) &= i^l \delta_{\mu m} 2\alpha^{l+5} \sqrt{\frac{n!(2l+1)}{\sqrt{\pi}[\Gamma(n+l+\frac{3}{2})]^3 l(l+1)}} (2n+l) \frac{1}{|\mathbf{k}|} e_p \frac{\hbar}{M_p} \Bigg\{ \\
&(l+1) \int_0^\infty dr r^{l+2} e^{-\alpha^2 r^2} L_n^{(l+\frac{1}{2})}(\alpha^2 r^2) j_l(|\mathbf{k}|r) \\
&-\frac{\hbar\alpha^2}{M_p c}(2n+l) \int_0^\infty dr r^{l+3} e^{-\alpha^2 r^2} L_n^{(l+\frac{1}{2})}(\alpha^2 r^2) j_{l+1}(|\mathbf{k}|r) \\
&+\frac{\hbar^2\alpha^2}{2M_p^2 c^2}(2n+l) l \int_0^\infty dr r^{l+2} e^{-\alpha^2 r^2} j_l(|\mathbf{k}|r) \\
&+\frac{\hbar^2\alpha^2}{2M_p^2 c^2}(2n+l) \int_0^\infty dr r^{l+3} e^{-\alpha^2 r^2} \frac{dL_n^{(l+\frac{1}{2})}(\alpha^2 r^2)}{dr} j_l(|\mathbf{k}|r) \Bigg\} \quad . \qquad (9)
\end{aligned}
$$

Summing over m of the final state and the two polaization of the photon, the El transition rate is

$$T(l;E) = \frac{1}{2l+1}\frac{|\mathrm{k}|}{2\pi\hbar c^2}\sum_{\mu=\pm1}\sum_{m=-l}^{l}\left|M_{fi}^{(H.O.)}(|\mathrm{k}|\mu;El)\right|^2 \quad . \tag{10}$$

3 Results

The El transition rates for the photon energies E_γ (values of $|\mathrm{k}|R$) are shown in Fig.1,3,5 (Fig.2,4,6). Solid lines are the results of the Weisskopf units for the El transitions. Points represent the strict El transition rates $T(l;E)$. The radius of nucleus is supposed as $R = 1.2\times A^{1/3}\mathrm{fm}$, where A indicates mass number. The Weisskopf units are continuous and large at high photon energies and heavy nuclear masses. However, the strict El transition rates $T(l;E)$ with the harmonic ocillator wave functions decrease with increasing photon energies and nuclear masses. And, $T(l;E)$ are discontinuous because the initial $1s$ state transmit disconnectedly to excited energy levels nl through the El transitions. The strict El transition rates $T(l;E)$ are approximately equal to the Weisskopf units in the case of low photon energies and $|\mathrm{k}|R \ll 1$. The differences between the strict transition rates and Weisskopf units increase with increasing photon energies and the values of $|\mathrm{k}|R$.

4 Discussions

The expression of the electric multipole field is not unique. For example, another form of the electric multipole field than Eq.(1) is

$$\mathbf{A}'_{l\mu}(\mathbf{r};E) = \sqrt{\frac{l+1}{l}}\frac{1}{|\mathbf{k}|}\nabla j_l(|\mathbf{k}|r)Y_{l\mu}(\Omega) - \sqrt{\frac{2l+1}{l}}j_{l+1}(|\mathbf{k}|r)\mathbf{Y}_{l\mu,l+1}(\Omega) \quad . \tag{11}$$

The El transition matrix (2) becomes

$$\begin{aligned} M'_{fi}(|\mathbf{k}|\mu;El) = \sqrt{2\pi}i^l\sqrt{2l+1}\Bigg\{ & \\ & \sqrt{\frac{l+1}{l}}\frac{E_f-E_i}{\hbar|\mathbf{k}|}e_p\int d^3r\psi_f^*(\mathbf{r},t)\psi_i(\mathbf{r},t)j_l(|\mathbf{k}|r)Y_{l\mu}(\Omega) \\ & +i\sqrt{\frac{2l+1}{l}}\frac{e_p\hbar}{2M_pi}\int d^3r\Big[\psi_f^*(\mathbf{r},t)\nabla\psi_i(\mathbf{r},t) - (\nabla\psi_f^*(\mathbf{r},t))\psi_i(\mathbf{r},t)\Big] \\ & \cdot j_{l+1}(|\mathbf{k}|r)\mathbf{Y}_{l\mu,l+1}(\Omega)\Bigg\}e^{-i\omega t} \end{aligned} \tag{12}$$

with the electric multipole field (11). Both El transition matrix elements M_{fi} (5) and M'_{fi} (12) must have same contributions to the El transition rates. The matrix element between $1s$ and

nl states of the harmonic oscillator wave functions with the electric multipole field (11) is

$$M'^{(H.O.)}_{fi}(|\mathbf{k}|\mu;El) = i^l\delta_{\mu m}2\alpha^{l+5}\sqrt{\frac{n!(2l+1)}{\sqrt{\pi}[\Gamma(n+l+\frac{3}{2})]^3 l(l+1)}}(2n+l)\frac{1}{|\mathbf{k}|}e_p\frac{\hbar}{M_p}\Bigg\{ (l+1)\int_0^\infty dr r^{l+2}e^{-\alpha^2r^2}L_n^{(l+\frac{1}{2})}(\alpha^2r^2)j_l(|\mathbf{k}|r) + \frac{\hbar}{2M_pc}(l+1)\int_0^\infty dr r^{l+2}e^{-\alpha^2r^2}\frac{dL_n^{(l+\frac{1}{2})}(\alpha^2r^2)}{dr}j_{l+1}(|\mathbf{k}|r)\Bigg\} \quad , \quad (13)$$

and the both El transition matrix elements of $1s \rightarrow nl$ with the spherical harmonic oscillator wave functions $M^{(H.O.)}$ (9) and $M'^{(H.O.)}$ (13) are equivalent.

However, if the nuclear states are the constant wave functions that are used in deriving the Weisskopf units (i.e. the ground state $\sqrt{3/R^3}Y_{00}(\theta,\phi)$ and excited state $\sqrt{3/R^3}Y_{lm}(\theta,\phi)$ vanishing outside nuclei), two types of the El transition rates calculated from M_{fi} (5) and M'_{fi} (12) are nearly equal at $|\mathbf{k}|R \ll 1$ but differ from each other larger and larger in increasing the values of the $|\mathbf{k}|R$. An origin of this trouble is that the continuity equation for the current (4) must not be used with the constant wave functions, because these wave functions are not the energy eigen states and do not have energy eigen values. Then, the spherical harmonic oscillator wave functions are used in this work.

The initial state is ground s-wave state ($1s$) in this work. However the initial states must be considered to be excited states, when the final states nl of the transition $1s \rightarrow nl$ are already filled with nucleons. The $E1$ transition rates of $3s \rightarrow np$ ($n \geq 3$) for the nuclei that has the mass number $A = 220$ indicate in Fig.1. Behavior of the transition rates of $3s \rightarrow np$ is similar to the transition rate of $1s \rightarrow np$, but the values of the transition rates of $3s \rightarrow np$ are larger than the transition rates of $1s \rightarrow np$ for high photon energies. When the energy of the photon is enough large, the nucleon is ejected from nuclei. The $E1$ transition rate $1s \rightarrow$ the spherical wave states ($l = 1$) of the free particle $\frac{i^l}{\hbar}\sqrt{\frac{2M_p|\mathbf{k}|}{\pi}}j_l(|\mathbf{k}|r)Y_{lm}(\theta,\phi)$ for mass number $A = 20$ nuclei is shown in Fig.1. For the photon enegies $E_\gamma \gtrsim 35MeV$, the transition probabilities of $1s \rightarrow$ the ejected nucleon are more dominant than the transition probabilities of $1s \rightarrow$ the nucleon bound by nuclei.

5 Summary

We treated the electric multipole fields strictly and formulized the El transition rates that are valid at not only $|\mathbf{k}|R \ll 1$ but $|\mathbf{k}|R \gtrsim 1$. The spherical harmonic oscillator wave functions are used as the nuclear states. The only $1s \rightarrow nl$ transition process is considered in this work. These simple evaluations of transition rates are expected to be convenient units of order-of-magnitude estimation for high photon's energy.

The El matrix element M'_{fi} was gotten with another form of the electric multipole field $\mathbf{A}'$ than the ordinarily used one $\mathbf{A}$. The matrix element M'_{fi} gives the same results as the ordinary matrix element M_{fi} with the harmonic oscillator wave functions. The M'_{fi} is profitable for numerical calculation efficiently becuase the M'_{fi} has simpler expression than M_{fi}.

The procedure for calculation of $1s \rightarrow nl$ transitions are possible to extend the $n'l' \rightarrow nl$ transition in a case of realistic subjects. We did not consider the magnetic transition rates yet. But, it is possible to extend the electric transition rates to the magnetic transitions with introducing the spin of the nucleon.

References

[1] J. Ryckebusch, et al., Nucl. Phys., **A476** (1988) 237-271.

[2] U. Deutschmann, et al., Nucl. Phys., **A411** (1983) 337-356.

[3] V.F.Weisskopf, Phys. Rev., **83** (1951) 1073.

[4] F.Partovi, Ann. Phys., **27** (1964) 79.

[5] H. Arenhövel, Z. Phys., **A302** (1981) 25.

[6] M. M. Giannini and G. Rico, Riv.Nuovo Cim., 8 (1985) 1.

Fig. 1. - $E1$ transition rates vs. photon energy E_γ at various mass number A. Solid lines are Weisskopf units. Each points are strict transition rates $T(l=1;E)$ for $1s \rightarrow 1p$, $1s \rightarrow 2p$, $\cdots$ in the order of increasing photon energies.

Fig. 2. - $E1$ transition rates vs. $|\mathbf{k}|R$ at various mass number A.

Fig. 3. - $E2$ transition rates vs. photon energy E_γ at various mass number A.

Fig. 4. - $E2$ transition rates vs. $|\mathbf{k}|R$ at various mass number A.

Fig. 5. - $E3$ transition rates vs. photon energy E_γ at various mass number A.

Fig. 6. - $E3$ transition rates vs. $|\mathbf{k}|R$ at various mass number A.

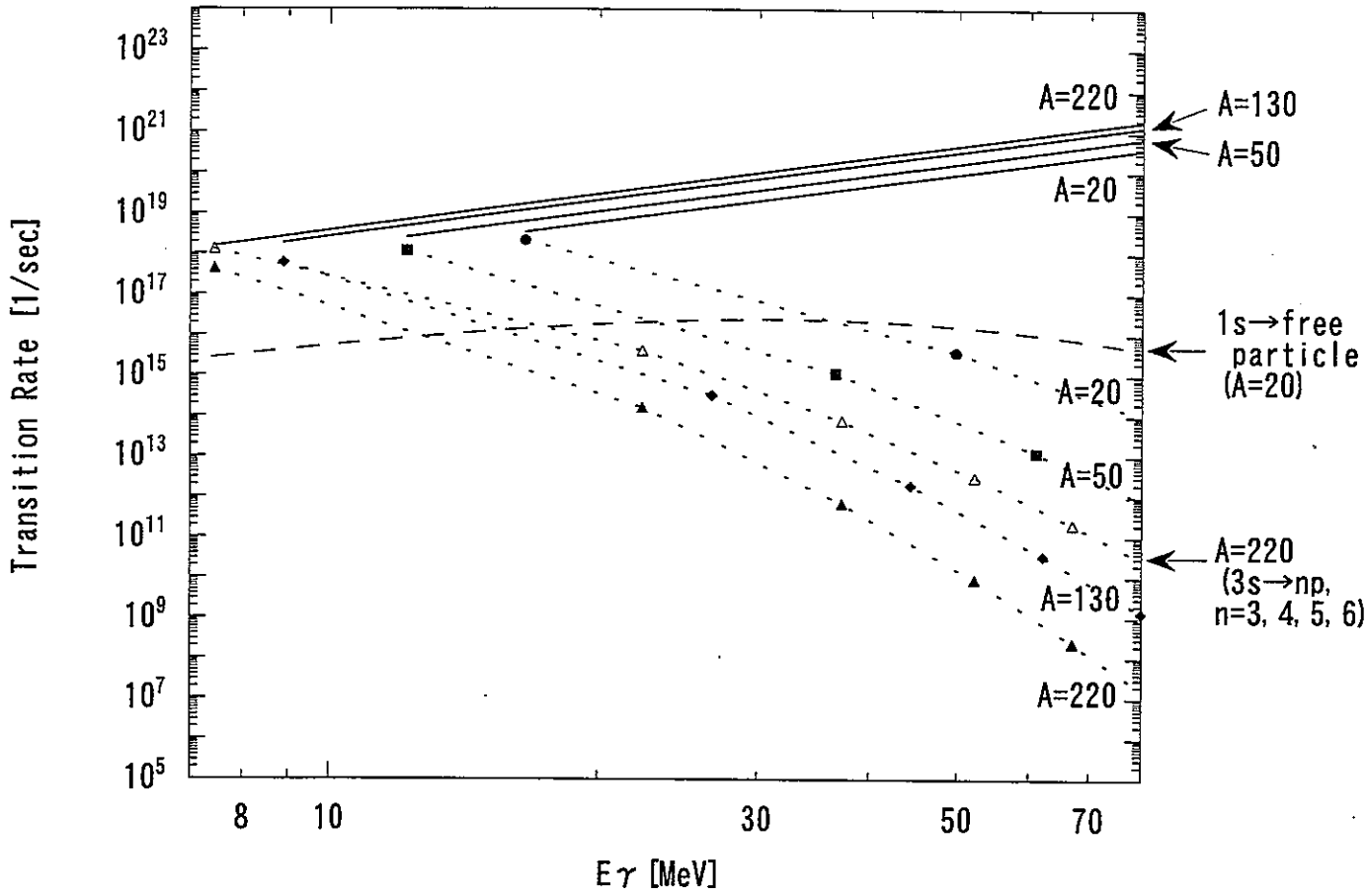

Fig. 1. E1 transition rate vs. photon energy at various mass number A. Solid lines are Weisskopf units. Each points are strict transition rates T(l=1;E) for 1s→1p, 1s→2p, … in the order of increasing photon energy.

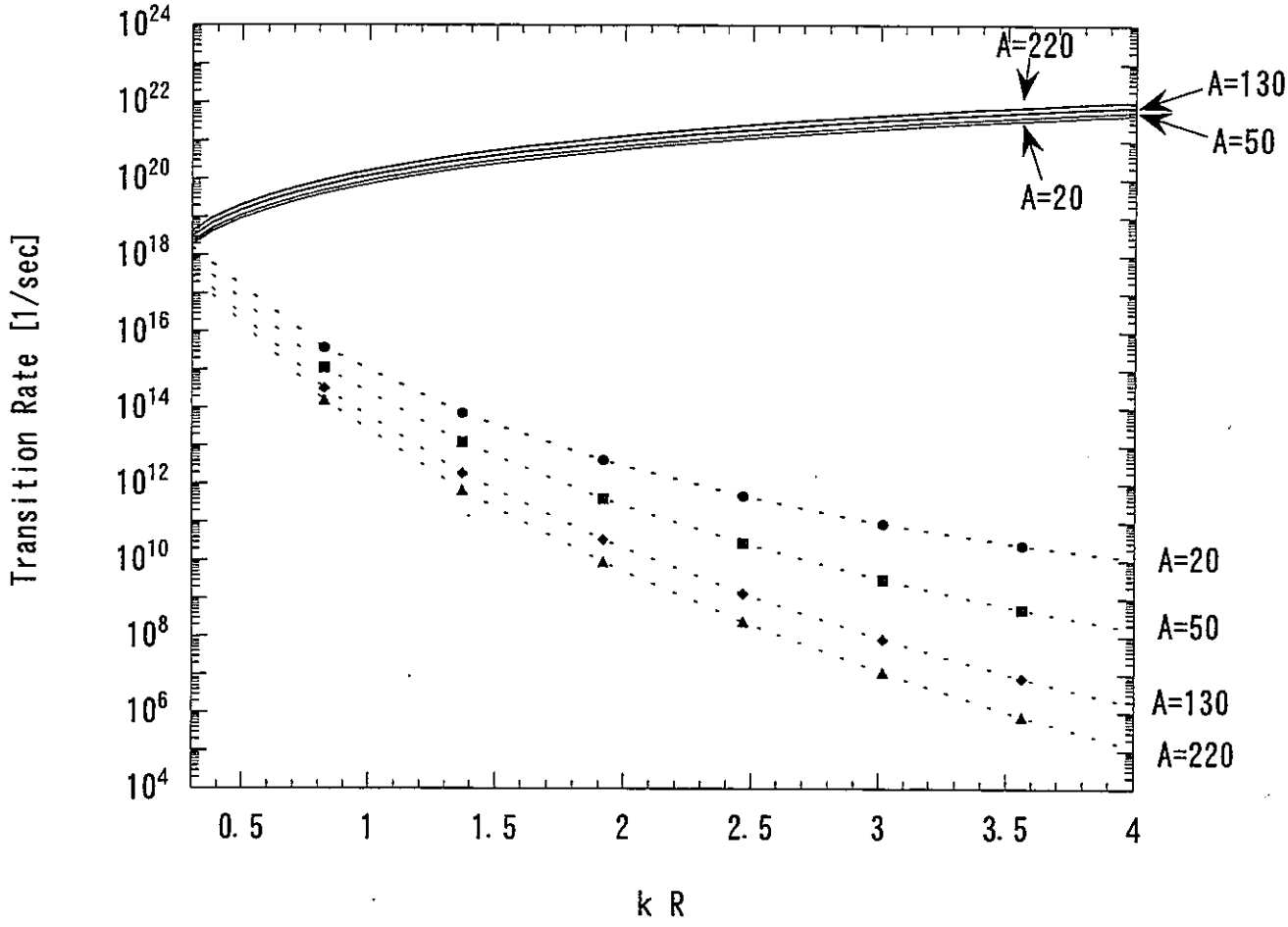

Fig2. E1 transition rate vs kR at various mass number A.

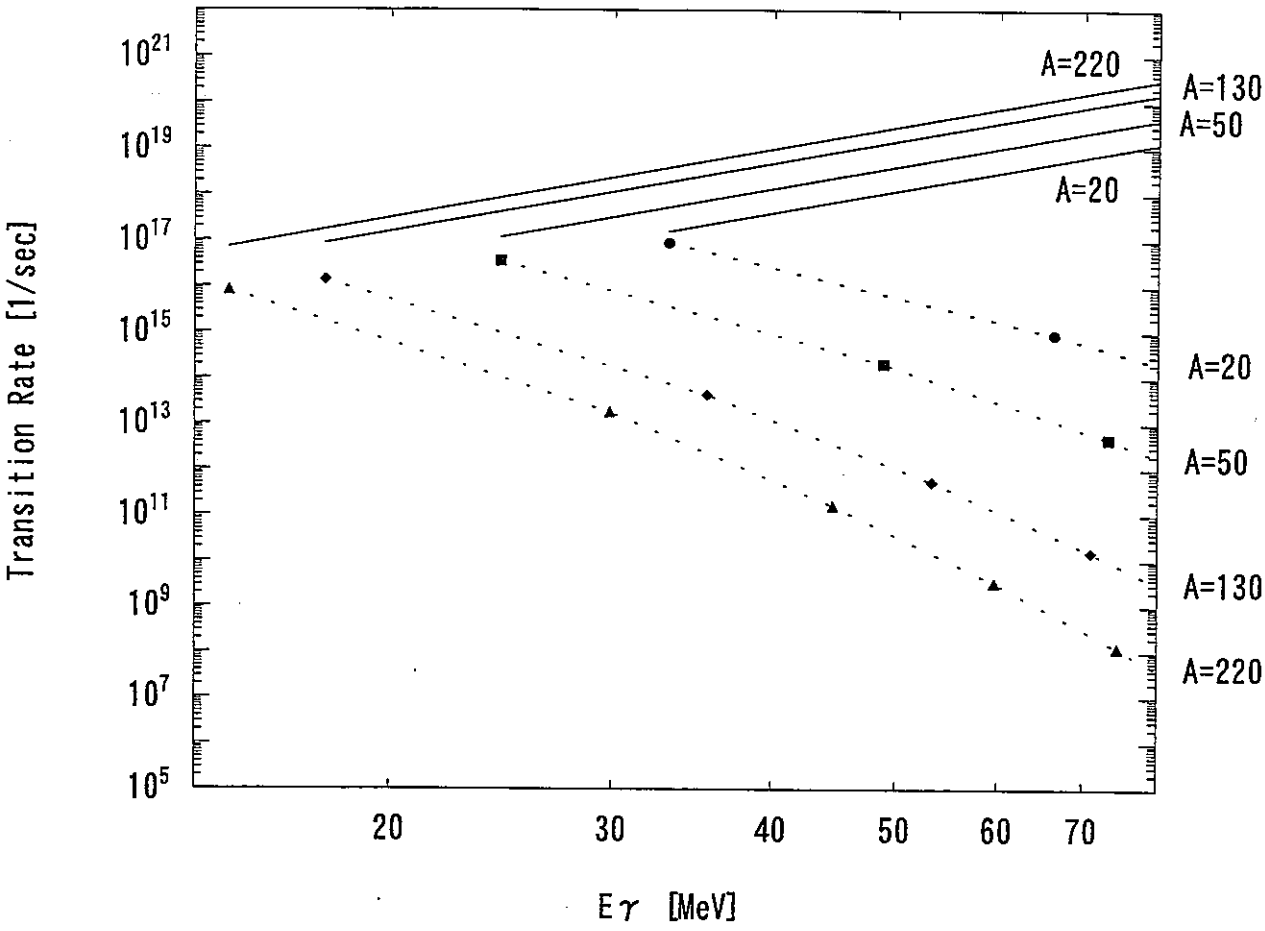

Fig3. E2 transition rate vs. photon energy.

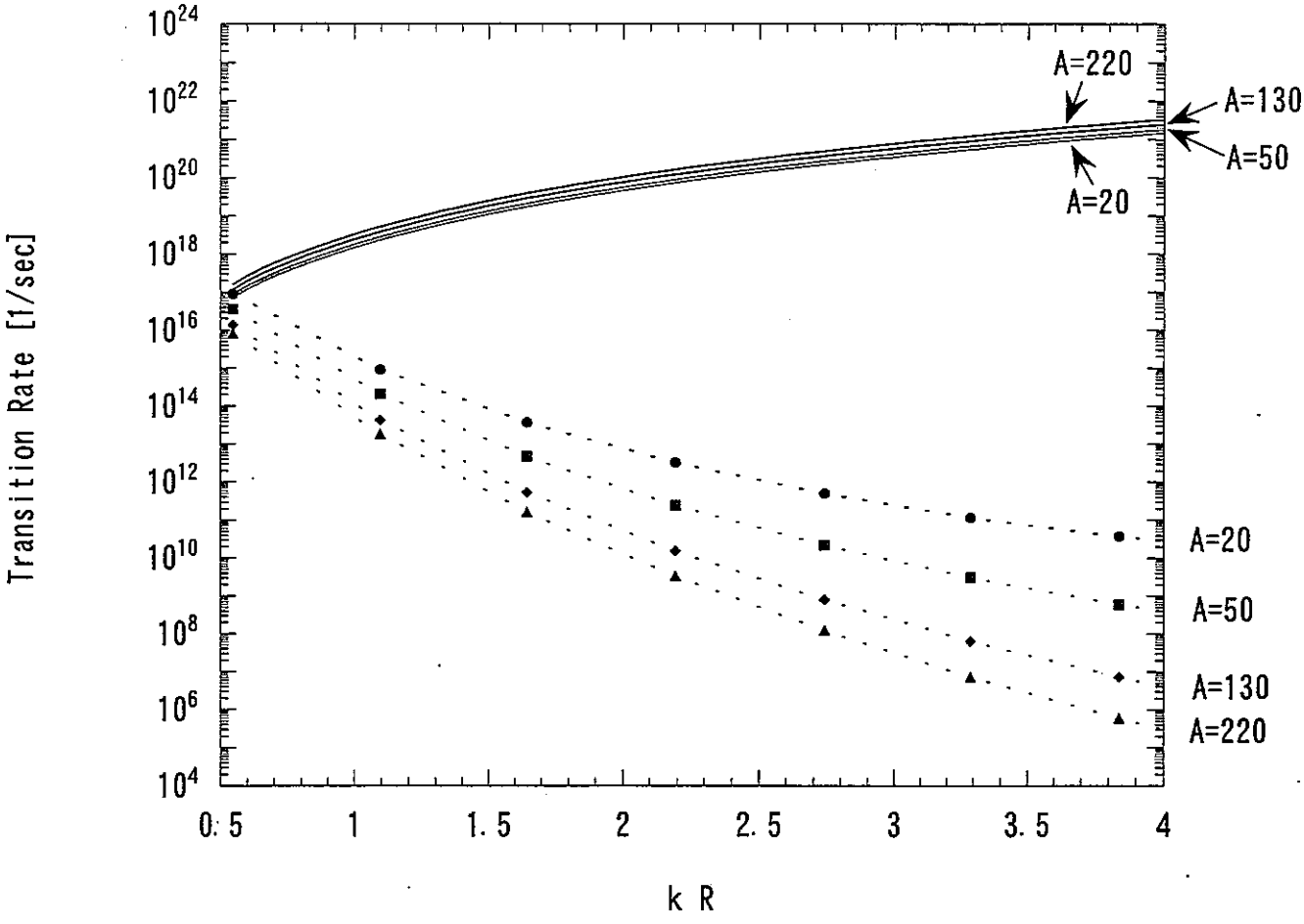

Fig. 4. E2 transition rate vs. kR.

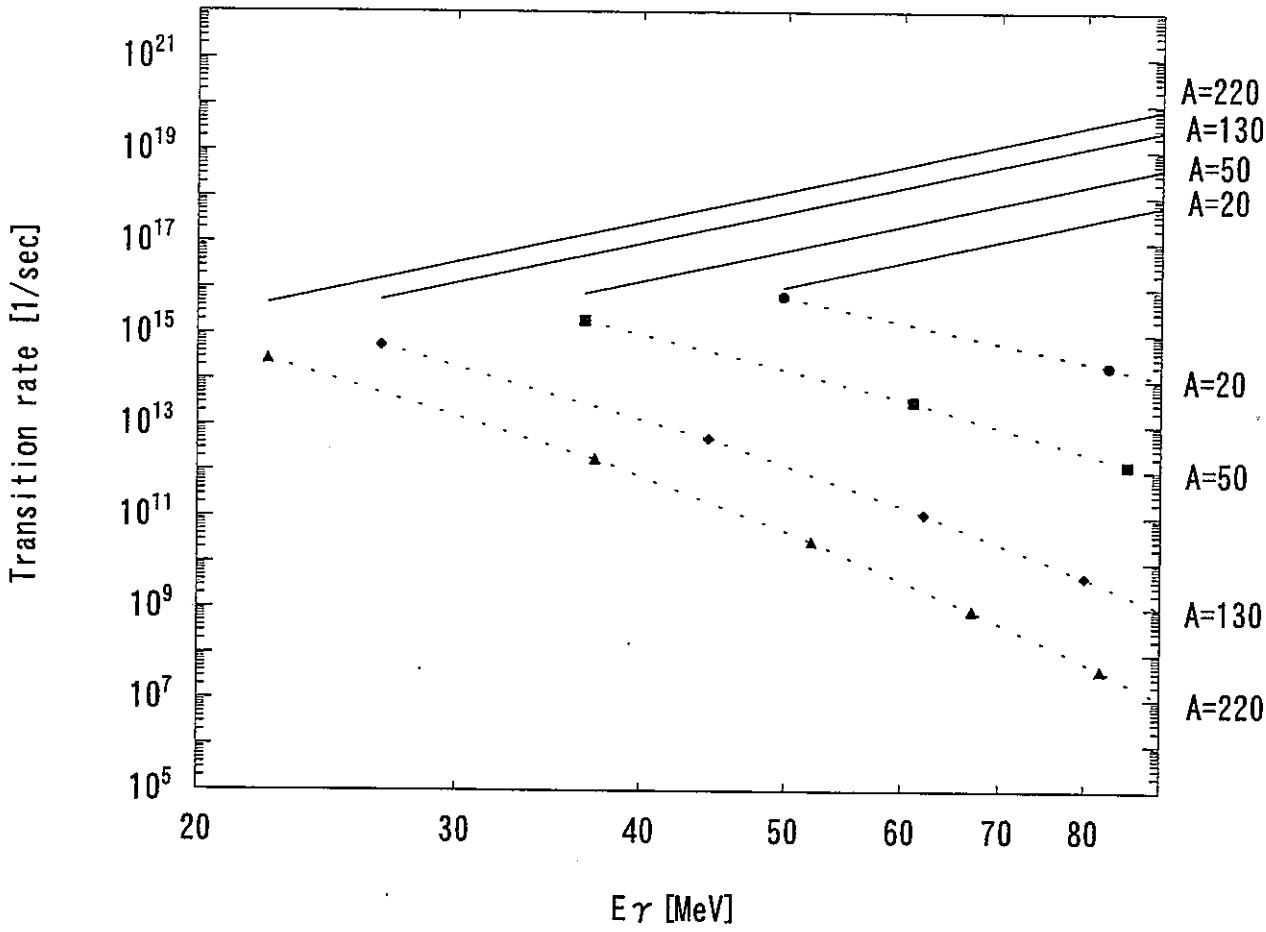

Fig. 5. E3 transition rate vs. photon energy.

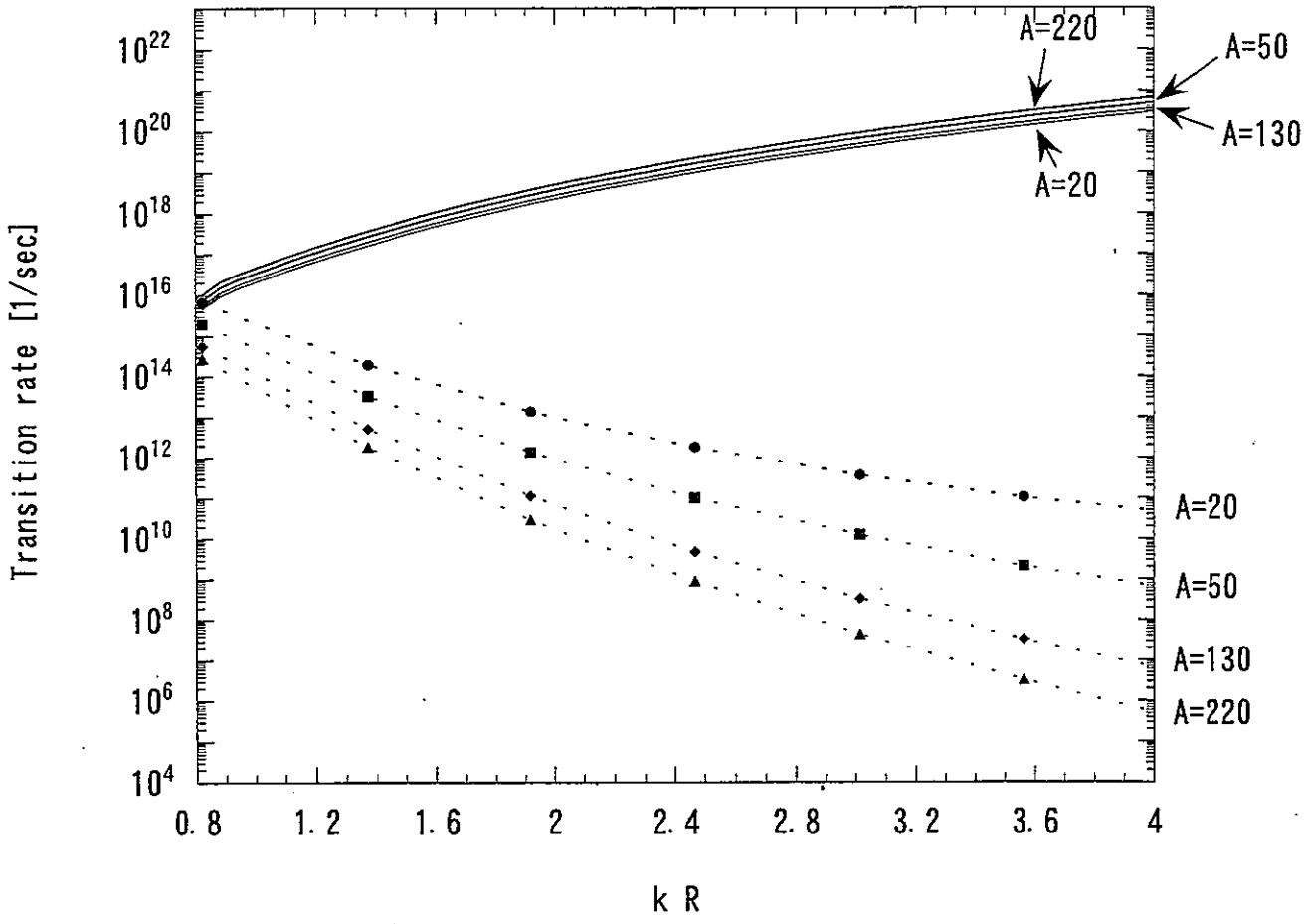

Fig. 6. E3 transition rate vs. kR.

2.2 Production of the isomeric state of ^{138}Cs in the thermal neutron capture reaction $^{137}Cs(n,\gamma)^{138}Cs$

Production of the isomeric state of ^{138}Cs in the thermal neutron capture reaction $^{137}Cs(n,\gamma)^{138}Cs$

Hiroaki WADA[*1], Shoji NAKAMURA[*1], Kazuyoshi FURUTAKA[*1], Toshio KATOH[*1,*2],

Hajimu YAMANA[*3], Toshiyuki FUJII[*3] and Hideo HARADA[*1]

[*1]*Tokai Works, Japan Nuclear Cycle Development Institute*

[*2]*Gifu College of Medical Technology*

[*3]*Research Reactor Institute, Kyoto University*

*1 *Tokai-mura, Naka-gun, Ibaraki-ken 319-1194.*

*2 *Nagamine, Ichihiraga, Seki-shi 501-3892.*

*3 *Kumatori-cho, Sennan-gun, Osaka-fu 590-0494*

In order to obtain precise data of the neutron capture cross section of the reaction $^{137}Cs(n,\gamma)^{138}Cs$, the production probability of isomer state ^{138m}Cs was measured in this work. Target of about 0.37MBq ^{137}Cs was irradiated for 3min. in the pneumatic tube facility (Pn-3) of Kyoto University Reactor (KUR). The 1436keV γ-ray emitted from both of ^{138g}Cs and ^{138m}Cs was measured. A production ratio of ^{138m}Cs to (^{138g}Cs and ^{138m}Cs) was deduced from time dependence of peak counts of 1436keV γ-ray by making use of difference of half-lives of ^{138g}Cs (33.41min.) and ^{138m}Cs (2.91min.). The probability of the production of ^{138m}Cs was obtained as 0.75 ± 0.18 and this value revised the effective cross section upwards 9 $\pm2\%$. The effective cross section $\hat{\sigma}$ and the thermal neutron capture cross section σ_0 were obtained as $\hat{\sigma}=0.29\pm0.02$ b and $\sigma_0=0.27\pm0.03$ b with taking into account the production of ^{138m}Cs.

KEYWORDS: neutron capture, cesium 137, cesium 138, isomer, thermal neutron, cross section, nuclear transmutation

放射性核種 ^{137}Cs の熱中性子吸収断面積を高精度化するため,$^{137}Cs(n,\gamma)^{138}Cs$ 反応で ^{138m}Cs (^{138}Cs のアイソマー)が生成される確率を測定し,^{138m}Cs 生成の寄与を含む断面積を求めた。照射試料は約 0.37MBq の ^{137}Cs を使い,京都大学原子炉実験所の圧気輸送管 Pn-3 で中性子を 3 分間照射した。^{138g}Cs(基底準位)と ^{138m}Cs の半減期がそれぞれ 33.41 分と 2.91 分と異なることを利用して,^{138g}Cs と ^{138m}Cs の両方の崩壊から放射される 1436keV γ 線の時間変化から,^{138g}Cs と ^{138m}Cs が熱中性子吸収反応で生成される割合を求めた。その結果,$^{137}Cs(n,\gamma)^{138}Cs$ 反応で生成される ^{138}Cs のうち,^{138m}Cs が生成される確率は 0.75±0.18 となった。この場合,^{138m}Cs 生成が熱中性子吸収断面積に与える寄与はこれまでの実験値を 9±2%上方修正させ,$^{137}Cs(n,\gamma)^{138}Cs$ 反応の熱中性子吸収断面積として σ_0=0.27±0.03 b (実効断面積は $\hat{\sigma}$=0.29±0.02 b)が得られた。

1. Introduction

Precise data of the neutron cross sections are extremely important for the study of the nuclear transmutation of the fission products. The ^{137}Cs is one of the important fission products because it has large fission yield. The thermal neutron capture cross section σ_0 of the reaction $^{137}Cs(n,\gamma)^{138}Cs$ was measured for the first time by Stupegia in 1960[1]. Stupegia's result ($\sigma_0=0.110\pm0.033$ b [1]) was obtained by an activation method with a NaI spectrometer. In 1990, the thermal neutron capture cross section was measured by using a high purity Ge detector and the obtained value was $\sigma_0=0.25\pm0.02$ b [2]-[3]. This result much reduced the error of the σ_0 value compared to that from Stupegia's result. However, the contribution of the isomeric state to the σ_0 value has never been included in the previous measurements. Both of the ground state ^{138g}Cs (the spin and parity are 3^-) and the isomer state ^{138m}Cs (the spin and parity are 6^-) are produced in the reaction $^{137}Cs(n,\gamma)^{138}Cs$ as shown in Fig. 1. There has been no experimental data of the probability of the production of ^{138m}Cs. In the previous works[2]-[3], the γ-rays of ^{138m}Cs were not measured because the half-life of ^{138m}Cs is so short as 2.91 min. Therefore, the probability of the production of ^{138m}Cs, x, was estimated in ref.3 by the calculation based on the Huizenga-Vandenbosch model[4]. The theoretically estimated value x is as small as 0.11 (or 0.34) if the spin parity of compound nuclei is 3^+ (or 4^+), and the value x revises the neutron cross section only upwards +1.2% (or +3.9%)[3].

A purpose of this work is to measure the probability of the production of ^{138m}Cs, x. To obtain the value of x experimentally, not only the 1436keV γ-ray emitted from ^{138g}Cs but also the 1436keV γ-ray of ^{138m}Cs were measured.

2. Experiments

The experiment was performed at Research Reactor Institute, Kyoto University.

The standardized radioactive $^{137}CsCl$ solution was obtained from Amersham Co. Because ^{38}Cl produced via $^{37}Cl(n, \gamma)^{38}Cl$ reaction emits 1643keV γ-rays, the removal of chlorine from the irradiation target was a significant procedure for the preparation of the target. The cesium chloride was changed to cesium nitrate as follows. The standardized solution was once dried by heating in a glass vial. Then, about 1*ml* of 3% nitric acid solution was added and the solution was heated to dryness. This procedure was repeated three times to convert the source to $^{137}CsNO_3$. The dried $^{137}CsNO_3$ was dissolved with 1*ml* of 3% nitric acid. 95 μl of this solution whose radioactivity was 0.37MBq of ^{137}Cs was transferred into a polyethylene tube with a capacity of 1*ml* and dried out. In order to avoid the production of the ^{41}Ar via the irradiation of ^{40}Ar contained in the air, the air in the tubes was substituted for helium, and the tubes were sealed. The samples were irradiated for 3 minutes in the pneumatic irradiation facility (Pn-3) of Kyoto University Reactor (KUR). The flux monitor wires, *Co/Al* and *Au/Al* alloys, were irradiated together. Because the polyethylene tubes contained a trace amount of chlorine, ^{38}Cl was produced via the irradiation of ^{37}Cl. Thus, after the irradiation, the $^{137}CsNO_3$ in the tube was quickly dissolved with 3% nitric acid and transferred into an unirradiated tube. This was performed within 2 minutes from the end of the irradiation, and then it was fed to γ-spectrometry.

The γ-rays emitted from the irradiated sample were measured with a high purity Ge detector. The performance of the Ge detector was characterized as a 90% relative efficiency to a 7.6cm×7.6cmϕ NaI(Tl) detector and 2.1keV FWHM at the 1.33MeV γ-peak of ^{60}Co. The energy dependence of peak efficiencies of the Ge detector were calibrated with a standard γ-ray source of ^{152}Eu. The pulse height data with 8k channels were stored in a hard disk of a personal computer at 60 sec intervals for about 15 min. from the beginning of the measurement. After about 15 min., the pulse height data were recorded at 600sec intervals. The details of the γ-ray measurement are described in ref. 2 and 3.

3. Analysis and Results

Fig. 2 and 3 show γ-ray spectra obtained from the irradiated ^{137}Cs sample. Fig. 2 shows γ-ray spectrum measured for 15 min. after 2.07 min. from the end of irradiation. Fig. 3 is γ-ray spectrum measured for 80min. after 17.8 min. from the end of irradiation. The 1436keV γ-ray of ^{138}Cs and the 662keV γ-ray of ^{137}Cs can be seen in the spectra. The 1436keV γ-ray is emitted from both of ^{138g}Cs and ^{138m}Cs. The time dependence of a ratio Y_p(1436keV)/Y_p(662keV) was extracted from the observed γ-ray spectra in order to obtain the probability of the production of ^{138m}Cs, x. The Y_p(1436keV) and Y_p(662keV) represent the peak counts of the 1436keV γ-ray of ^{138}Cs and the 662keV γ-ray of ^{137}Cs, respectively. The ratio Y_p(1436keV)/Y_p(662keV) does not depend on the amounts of ^{137}Cs contained in each target. The correction of the dead time is also made automatically by using the ratio in the analysis. Fig.4 shows the behavior of the ratio Y_p(1436keV)/Y_p(662keV). The solid line is a curve $A_1 \exp(-\lambda_{138m}t) + A_2 \exp(-\lambda_{138g}t)$ fitted to experimental data, where λ_{138m} and λ_{138g} are the decay constants of ^{138m}Cs and ^{138g}Cs, respectively. The data of λ_i are listed in Table 1[6]. The coefficients A_1 and A_2 are free parameters. The values of A_1 and A_2 in each of ten runs are listed in Table 2. By averaging the results of ten runs, the coefficients were determined as $A_1=(2.68\pm0.35)\times10^{-4}$ and $A_2=(2.24\pm0.03)\times10^{-4}$.

The probability of the production of ^{138m}Cs, x, was deduced from the coefficients A_1 and A_2 as follows. While irradiation is performed, numbers of ^{137}Cs, ^{138m}Cs and ^{138g}Cs nuclei are given by equations as

$$\frac{dN_{137}}{dt} = -\lambda_{137}N_{137} - RN_{137} \quad , \tag{1}$$

$$\frac{dN_{138m}}{dt} = -\lambda_{138m}N_{138m} + xRN_{137} \quad , \tag{2}$$

$$\frac{dN_{138g}}{dt} = -\lambda_{138g}N_{138g} + (1-x)RN_{137} + (1-y)\lambda_{138m}N_{138m} \quad . \tag{3}$$

The N_{137} represents the number of ^{137}Cs nuclei contained in a ^{137}Cs sample. The value of N_{137} is almost invariant during the irradiation. The N_{138m} and N_{138g} are the numbers of ^{138m}Cs and ^{138g}Cs nuclei. The R is the reaction rate of the reaction $^{137}Cs(n,\gamma)^{138}Cs$. The y represents the intensity of the β^- decay from ^{138m}Cs. The λ_{137} is the decay constant of ^{137}Cs. From Equations (1)-(3), the numbers of ^{138m}Cs and ^{138g}Cs nuclei produced during the irradiation, N^0_{138m} and N^0_{138g}, are represented as

$$N^0_{138m} = \frac{xRN_{137}}{\lambda_{138m}}\left[1-\exp(-\lambda_{138m}T_{irr})\right] \tag{4}$$

and

$$N^0_{138g} = \frac{(1-xy)RN_{137}}{\lambda_{138g}}\left[1-\exp(-\lambda_{138g}T_{irr})\right] + \frac{x(1-y)RN_{137}}{\lambda_{138m}-\lambda_{138g}}\left[\exp(-\lambda_{138m}T_{irr})-\exp(-\lambda_{138g}T_{irr})\right] \quad . \tag{5}$$

The irradiation time T_{irr} is 180 sec in the experiments. After the end of irradiation, numbers of ^{137}Cs, ^{138m}Cs and ^{138g}Cs are given by

$$\frac{dN_{137}}{dt} = -\lambda_{137}N_{137} \quad , \tag{6}$$

$$\frac{dN_{138m}}{dt} = -\lambda_{138m}N_{138m} \quad , \tag{7}$$

$$\frac{dN_{138g}}{dt} = -\lambda_{138g}N_{138g} + (1-y)\lambda_{138m}N_{138m} \quad . \tag{8}$$

The peak counts Y_p(1436keV) and Y_p(662keV) can be calculated by using the equations (4)-(8). The ratio Y_p(1436keV)/Y_p(662keV) is expressed by the function $A_1\exp(-\lambda_{138m}t) + A_2\exp(-\lambda_{138g}t)$, and the coefficients A_1 and A_2 are represented as

$$A_1 = \frac{\varepsilon_p(1436\text{keV})\left[I_{\gamma m}(1436\text{keV}) - \frac{(1-y)\lambda_{138g}}{\lambda_{138m}-\lambda_{138g}}I_{\gamma g}(1436\text{keV})\right]\lambda_{138m}N^0_{138m}}{\varepsilon_p(662\text{keV})I_\gamma(662\text{keV})\lambda_{137}N_{137}} \tag{9}$$

and

$$A_2 = \frac{\varepsilon_p(1436\text{keV})I_{\gamma g}(1436\text{keV})\left[\lambda_{138g}N^0_{138g} + \frac{(1-y)\lambda_{138m}\lambda_{138g}}{\lambda_{138m}-\lambda_{138g}}N^0_{138m}\right]}{\varepsilon_p(662\text{keV})I_\gamma(662\text{keV})\lambda_{137}N_{137}} \quad . \qquad (10)$$

The $I_{\gamma m}(1436\text{keV})$ and $I_{\gamma g}(1436\text{keV})$ are emission probabilities of 1436keV γ-ray emitted from ^{138m}Cs and ^{138g}Cs, respectively. The $I_\gamma(662\text{keV})$ is the emission probability of 662keV γ-ray emitted from ^{137}Cs. The data of λ_i, I_i and y are listed in Table 1[6]. The ε_p (662keV) and ε_p (1436keV) are detection efficiency of 662keV and 1436keV γ-ray, respectively. From Equations (4,5,9,10), the probability of the production of ^{138m}Cs, x, is represented as

$$x = \frac{\frac{A_1}{A_2}}{\left(\frac{I_{\gamma m}(1436\text{keV})}{I_{\gamma g}(1436\text{keV})} - \frac{(1-y)\lambda_{138g}}{\lambda_{138m}-\lambda_{138g}}\right)\frac{1-\exp(-\lambda_{138m}T_{irr})}{1-\exp(-\lambda_{138g}T_{irr})} - \frac{A_1}{A_2}\left(\frac{(1-y)\lambda_{138g}}{\lambda_{138m}-\lambda_{138g}} - y\right)} \quad . \qquad (11)$$

For the averaged values $A_1=(2.68\pm0.35)\times10^{-4}$ and $A_2=(2.24\pm0.03)\times10^{-4}$, the probability of the production of ^{138m}Cs was obtained as $x = 0.75\pm0.18$. It is noticed that the value of x is much larger than the theoretically estimated value $x = 0.11$ or 0.34 [3].

From Equations (4,5,10), the reaction rate is expressed as

$$R = \frac{A_2\varepsilon_p(662keV)I_\gamma(662keV)\lambda_{137}}{\varepsilon_p(1436keV)I_{\gamma g}(1436keV)\left[1+x\left(\frac{(1-y)\lambda_{138g}}{\lambda_{138m}-\lambda_{138g}} - y\right)\right]\left[1-\exp(-\lambda_{138g}T_{irr})\right]} \quad . \qquad (6)$$

The values of the reaction rates in each of ten runs are listed in Table 2. The neutron flux were measured in four runs by the flux monitors (*Co/Al* and *Au/Al* alloys) in Westcott convention[5]. Simplified neutron flux notations, ϕ_1 and ϕ_2, are defined as $\phi_1 \equiv nv_0$ and $\phi_2 \equiv nv_0 r(T/T_0)^{1/2}$. The n is the neutron density including thermal and epithermal neutron. The neutron velocity v_0 is 2,200 m/s. The r is a measure of the relative density of epithermal neutrons. The T and T_0 are the neutron temperature and 293.6K, respectively. The quantity $r(T/T_0)^{1/2}$ gives the fraction of epithermal neutron in the neutron spectrum. Values of the simplified flux ϕ_1 and ϕ_2 at the ^{137}Cs sample position are summarized in Table 3. The

effective cross section $\hat{\sigma} = R/(nv_0) = R/\phi_1$ was obtained as $\hat{\sigma}$ =0.30±0.02 b in the present measurement.

4. Disscussion

The inclusion of the feeding from the isomeric state (x= 0.75±0.18) revises the neutron cross section upwards 9±2%. The effective cross section of the previous work[(2)-(3)] increases as $\hat{\sigma}$ = 0.29±0.02 b after taking into account the production of ^{138m}Cs. The present measurement ($\hat{\sigma}$ =0.30 ± 0.02 b) and the revised result from the previous measurement ($\hat{\sigma}$ = 0.29±0.02 b) agree within the limits of the errors. Therefore, the weighted average value $\hat{\sigma}$ = 0.29±0.02 b is recommended as the effective capture cross section. The capture cross section σ_0 for 2,200 m/s neutrons is 0.27±0.03 b after taking into account the isomer production.

The decay branch of ^{138m}Cs to ^{138}Ba via β^- decay, y, is 0.19±0.02[(6)-(8)] and the error of y is as large as 11%. Fig.5 shows that the allowed value of x varies as $0.56 \leq x \leq 1$ in the region of y=0.19±0.02 [(6)-(8)]. The error of y has a great influence on the value of x. However, the uncertainties of σ_0 and $\hat{\sigma}$ due to the error of y are small (about 3%). In order to make the uncertainty of x small, the value of the intensity of the β^- decay from ^{138m}Cs, y, must be measured accurately. If the intensity of isomeric transition, (1-y), can be measured accurately, the value of y will be known accurately. In the present measurement, 79.9keV γ-ray emitted by the isometric transition was not detected because emission probability of 79.9keV γ-ray is small (0.369±0.010%[(6)]).

5. Conclusion

In order to determine the probability of the production of ^{138m}Cs, x, in the reaction $^{137}Cs(n,\gamma)^{138}Cs$, the variation of the count of the 1436keV γ-ray with time was measured.

The experimental result of x was 0.75 ± 0.18 and this was much larger than the theoretically estimated value x = 0.11 or 0.34. For the value of $x = 0.75 \pm 0.18$, the value of the effective cross section is revised upwards $9 \pm 2\%$. The effective cross section $\hat{\sigma}$ and the thermal cross section σ_0 of the reaction $^{137}Cs(n,\gamma)^{138}Cs$ were obtained as $\hat{\sigma} = 0.29 \pm 0.02$ b and $\sigma_0 = 0.27 \pm 0.03$ b, respectively.

The decay data, the production of isomeric state ^{138m}Cs, significantly affects the neutron cross section data of the reaction $^{137}Cs(n,\gamma)^{138}Cs$. In order to obtain precise data of neutron cross section using activation method, studies of the decay data are important as shown in this case.

Acknowledgement

This work performed by using facilities of the Research Reactor Institute, Kyoto University (KUR). The authors wish to acknowledge their indebtedness to Mr. S. Nishikawa, Mr. K. Miyata and Mr. H. Kodaka of KUR for their help in the sample irradiation. The cooperation of the crew of KUR is appreciated very much. Thanks are also due to Prof. Y. Moriyama of Kyoto University and Dr. S. Nomura and Dr. T. Baba for their interest in and encouragement of this work.

References

(1) Stupegia, D. C. : *J. Nucl. Energy*, **12**, 16 (1960).

(2) Harada, H., *et al.* : *J. Nucl. Sci. Technol.*, **27**, 577 (1990).

(3) Sekine, T., *et al.* : *J. Nucl. Sci. Technol.*, **30**, 1099 (1993).

(4) Huizenga, J. R., Vandenbosch, R. V. : *Phys. Rev.*, **120**, 1305 (1960).

(5) Westcott, C. H., Walker, W. H., Alexander, T. K.: *Proc. 2nd Geneva Conf.*, Vol.16, p.70 (1958).

(6) Firestone, R. B., Shirley, V. S.: *Table of Isotopes*, (8th ed.), (1996), John Wiley & Sons, New York.

(7) Carraz, L. C., Monnand, E., Moussa, A.: *Nucl. Phys.*, **A171**, 209 (1971).

(8) Aumann, D. C., Weismann, D.: *J. Inorg. Nucl. Chem.*, **40**, 1611 (1978).

Table 1 The data used in the calculation[6].

parameters	data
λ_{138m}	ln2 / (2.91±0.08 min)
λ_{138g}	ln2 / (33.41±0.18 min)
I_γ(662keV)	0.851±0.002
$I_{\gamma m}$(1436keV)	0.19±0.02
$I_{\gamma g}$(1436keV)	0.763±0.016
y	0.19±0.02

Table 2 The coefficients A_1 and A_2, and the reaction rates.

Target No.	A_1 ($\times 10^{-4}$)	A_2 ($\times 10^{-4}$)	R ($\times 10^{-12}$) [1/sec]
1	2.37±1.39	2.13±0.14	5.02±0.38
2	2.85±1.12	2.19±0.11	5.23±0.30
3	2.98±1.04	2.22±0.11	5.32±0.29
4	2.68±1.20	2.49±0.11	5.85±0.31
5	0.65±1.08	2.50±0.11	5.54±0.30
6	4.01±1.09	2.06±0.10	5.15±0.29
7	2.74±1.03	2.10±0.11	5.02±0.29
8	3.24±1.10	2.31±0.11	5.55±0.30
9	2.24±1.05	2.20±0.11	5.15±0.29
10	2.92±1.06	2.19±0.11	5.24±0.29
Average	2.68±0.35	2.24±0.03	5.31±0.18

Table 3 The neutron flux determined by Westcott convention.

Run No.	ϕ_1 [n/cm^2 sec]	ϕ_2 [n/cm^2 sec]
1	$(1.65 \pm 0.01) \times 10^{13}$	$(6.64 \pm 0.08) \times 10^{11}$
4	$(1.83 \pm 0.01) \times 10^{13}$	$(5.07 \pm 0.06) \times 10^{11}$
6	$(1.64 \pm 0.00) \times 10^{13}$	$(4.89 \pm 0.05) \times 10^{11}$
8	$(1.85 \pm 0.00) \times 10^{13}$	$(4.42 \pm 0.05) \times 10^{11}$
Average	$(1.75 \pm 0.11) \times 10^{13}$	$(5.00 \pm 0.03^{+1.65}_{-0.58}) \times 10^{11}$

Fig. 1 Process of $^{137}Cs(n, \gamma)^{138}Cs$ reaction and decay scheme of ^{137}Cs, ^{138g}Cs and ^{138m}Cs.

Fig. 2 γ-ray spectrum obtained for irradiated ^{137}Cs sample.
(Measurement was started at 2.07 min. after irradiation and the counting period was 15 min.)

Fig. 3 γ-ray spectrum obtained for irradiated ^{137}Cs sample.
(Measurement was started at 17.8 min. after irradiation and the counting period was 80 min.)

Fig. 4 The time dependence of the ratio Y_p(1436keV)/Y_p(662keV).

Fig. 5 The dependence of the value of x on the value of y.

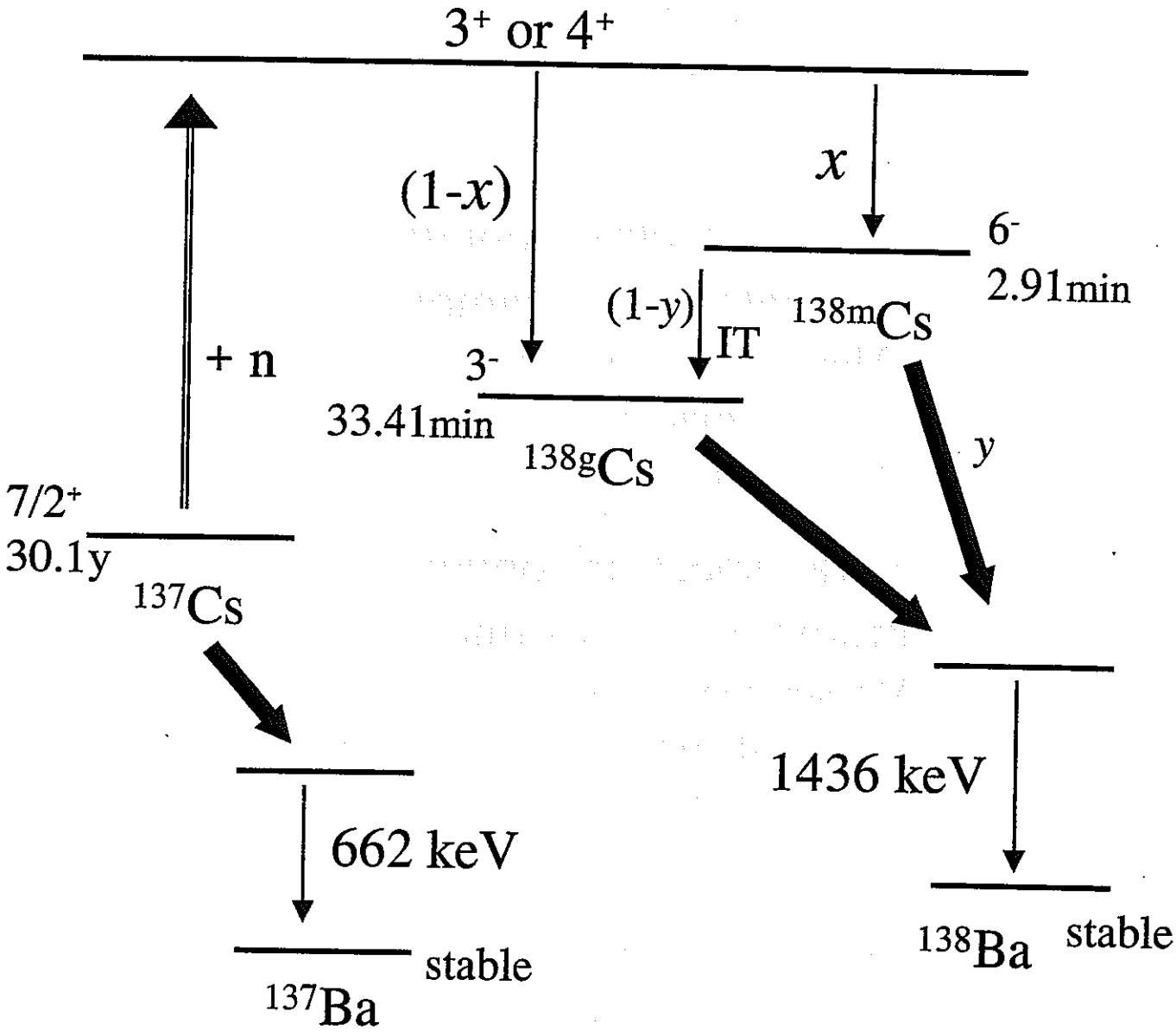
3+ or 4+
(1-x)
x
6-
2.91min
(1-y)
IT
138mCs
+ n
3-
33.41min
138gCs
y
7/2+
30.1y
137Cs
1436 keV
662 keV
stable
137Ba
138Ba
stable

Fig. 1

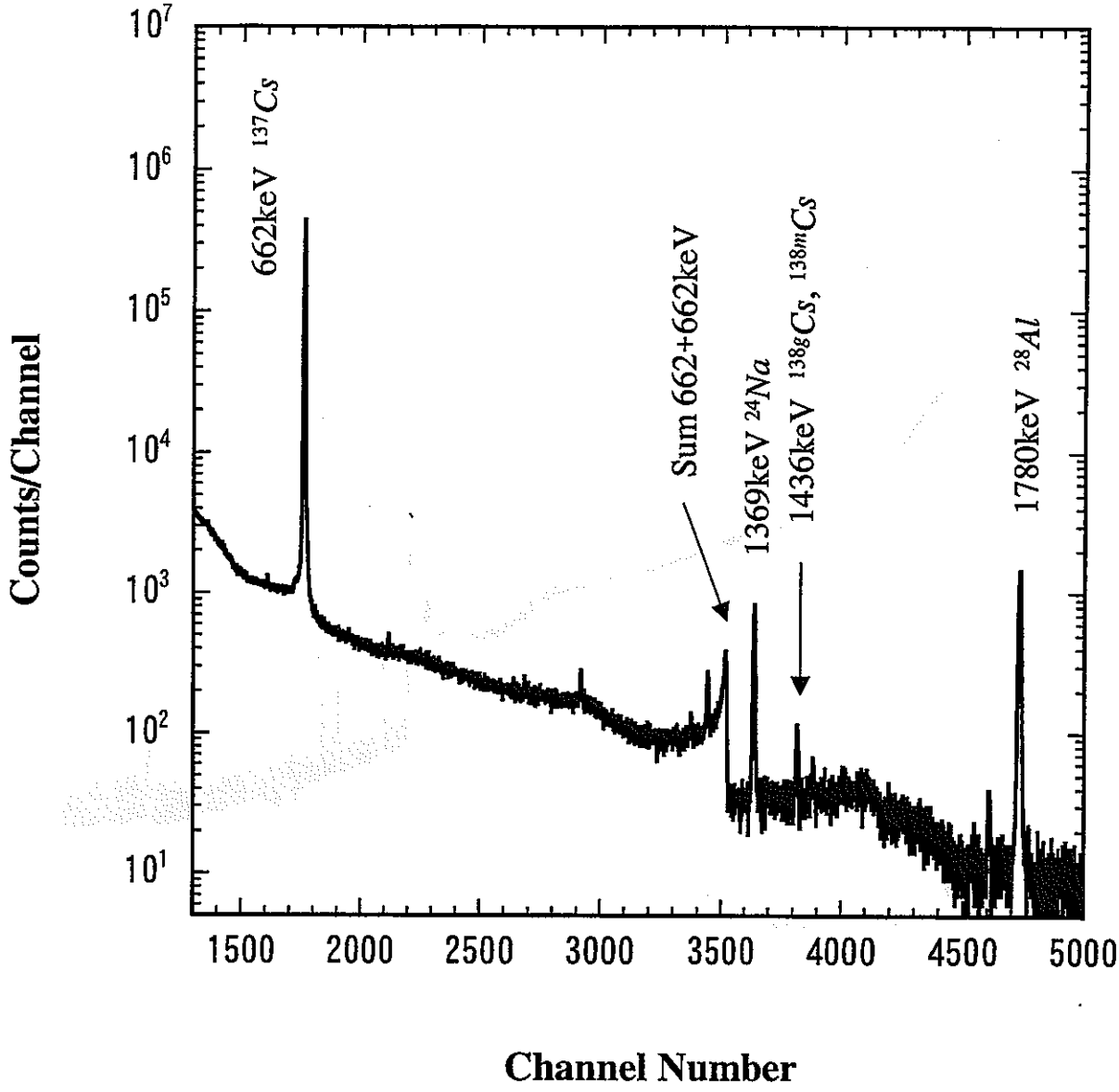
Counts/Channel
10^7
10^6
10^5
10^4
10^3
10^2
10^1
662keV ^{137}Cs
Sum 662+662keV
1369keV ^{24}Na
1436keV ^{138g}Cs, ^{138m}Cs
1780keV ^{28}Al
1500
2000
2500
3000
3500
4000
4500
5000
Channel Number

Fig. 2

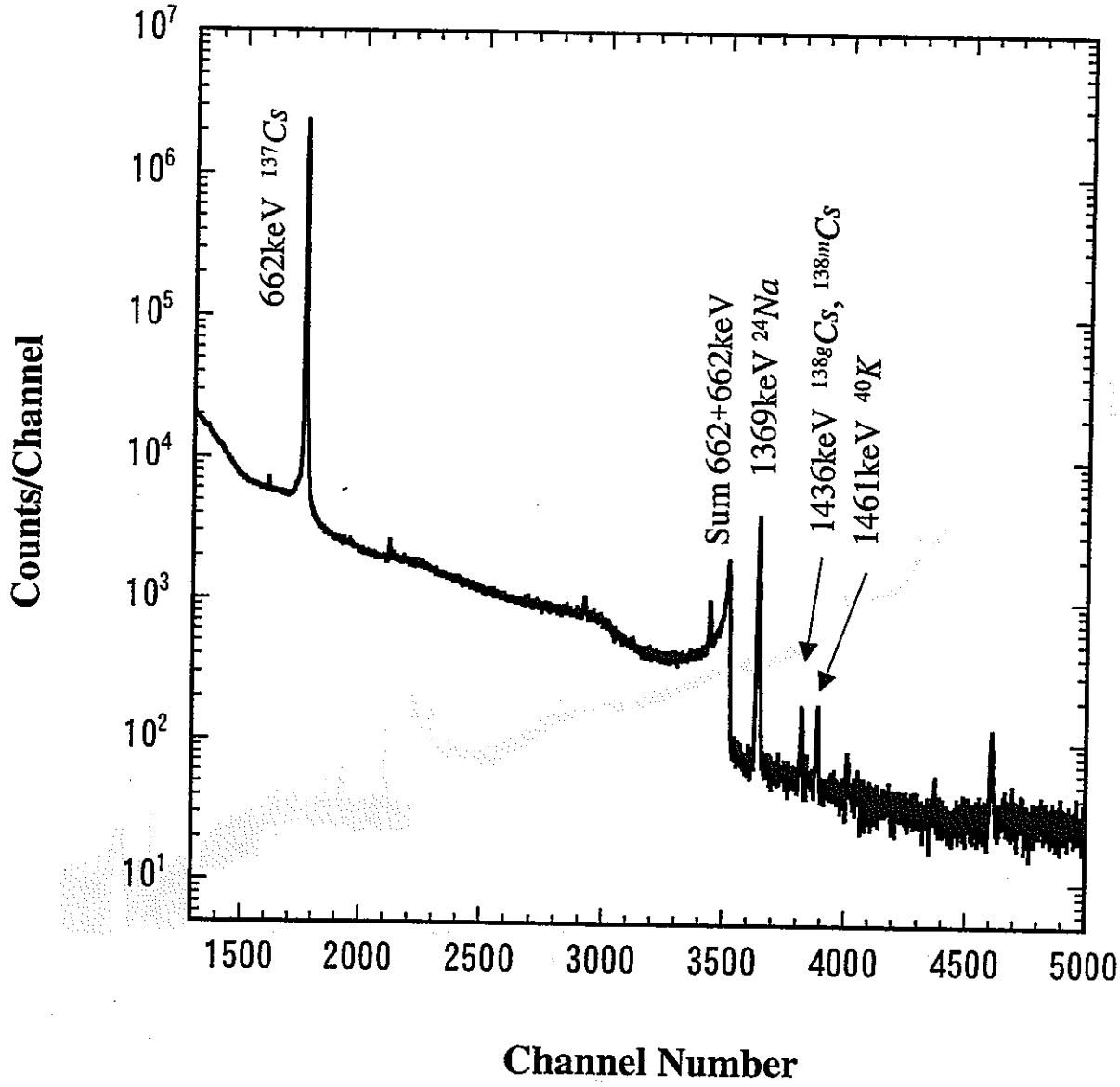
Counts/Channel
Channel Number
662keV 137Cs
Sum 662+662keV
1369keV 24Na
1436keV 138gCs, 138mCs
1461keV 40K

Fig. 3

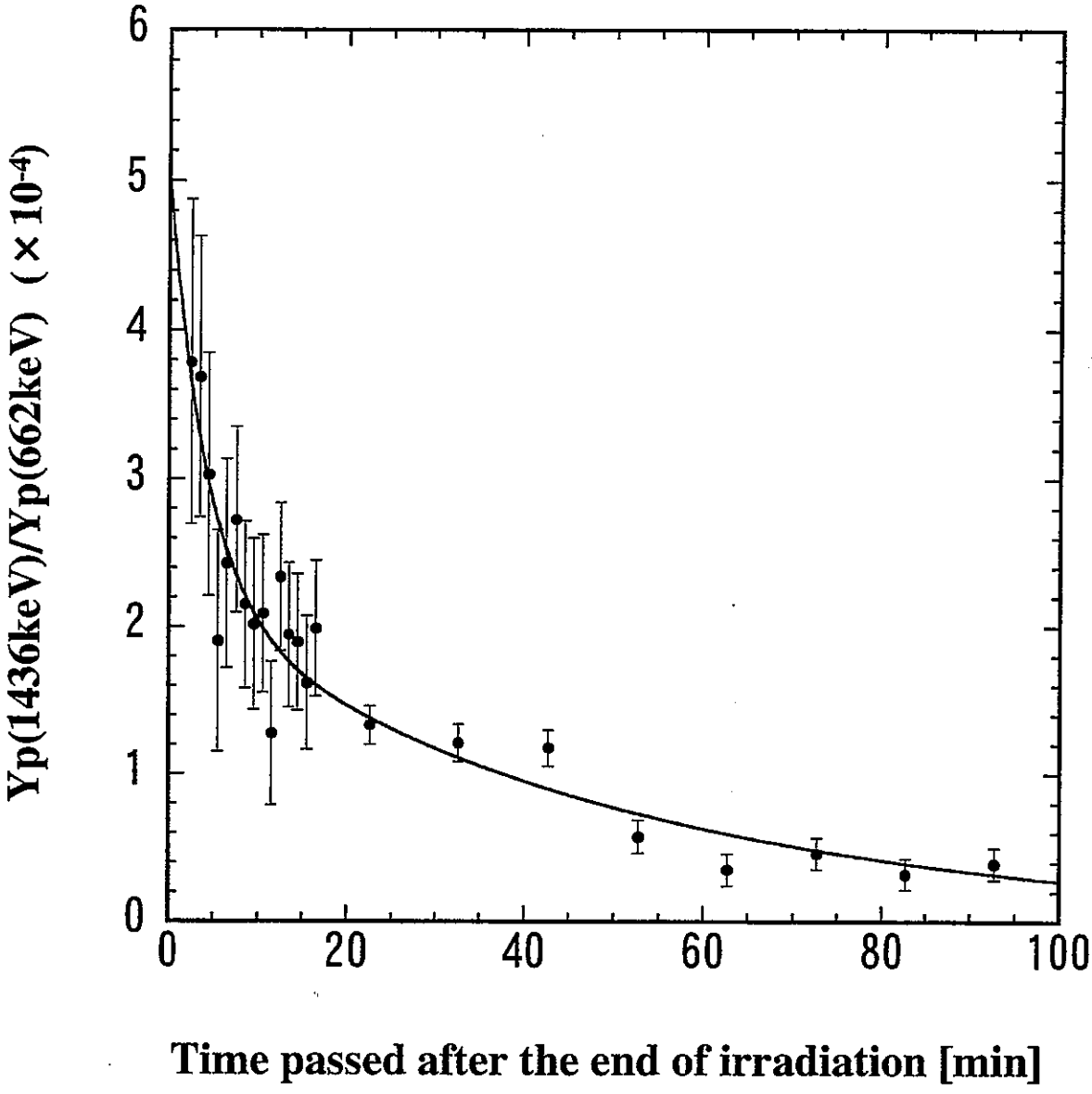
Yp(1436keV)/Yp(662keV) (×10-4)
0
1
2
3
4
5
6
0
20
40
60
80
100
Time passed after the end of irradiation [min]

Fig. 4

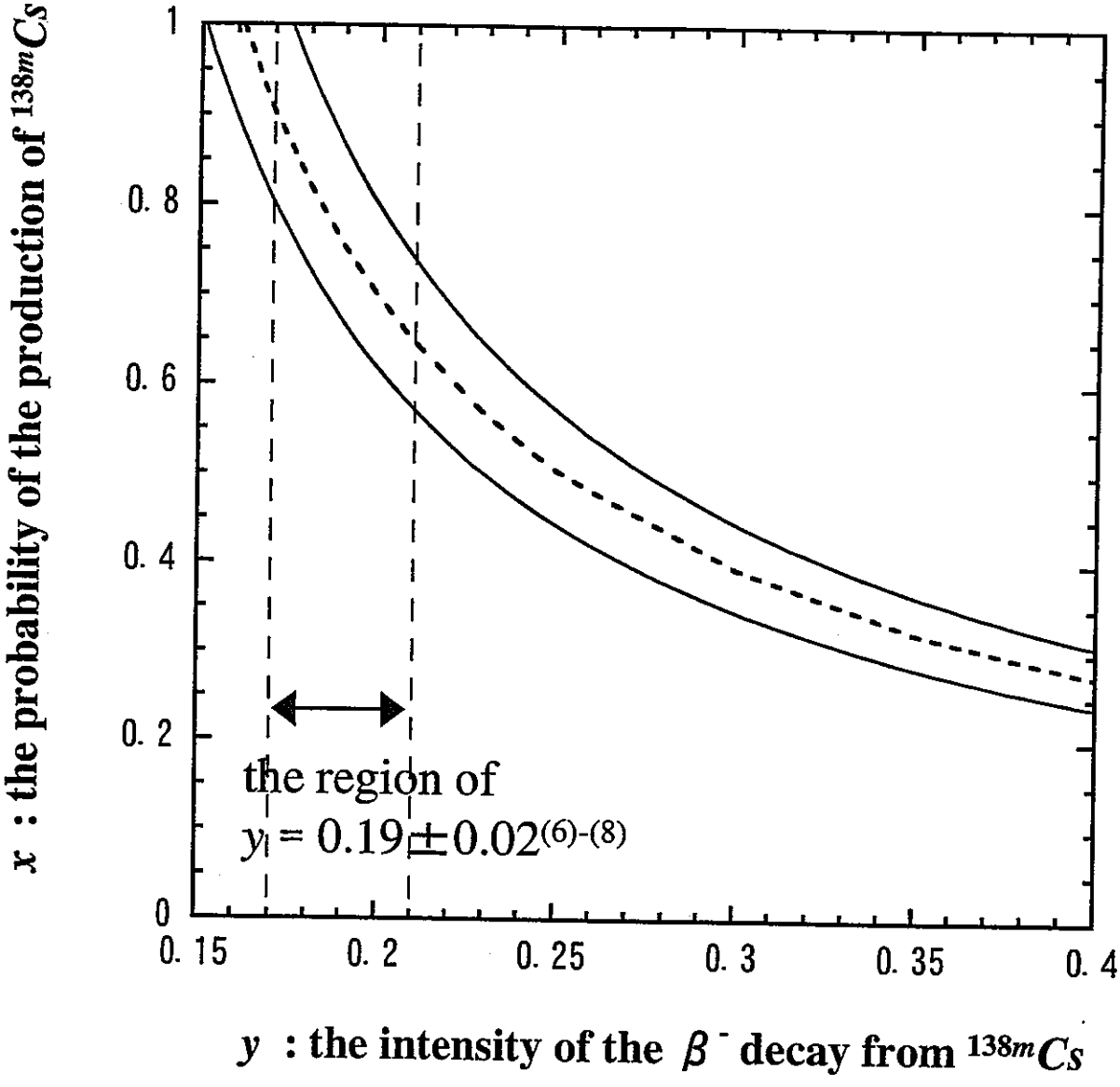
x : the probability of the production of 138mCs
1
0. 8
0. 6
0. 4
0. 2
0
0. 15
0. 2
0. 25
0. 3
0. 35
0. 4
the region of
y = 0.19±0.02(6)-(8)
y : the intensity of the β⁻ decay from 138mCs

Fig. 5

謝 辞

本研究を行なう際に，核燃料サイクル開発機構先進リサイクル解析評価 Gr の皆様に大変御世話になりました。とくに、原田秀郎氏は筆者を懇切に指導してくださいました。ここに深く感謝いたします。